Atmospheric Environment 84 (2014) 275–288

Contents lists available at ScienceDirect

Atmospheric Environment

journal homepage: www.elsevier.com/locate/atmosenv

Estimates of background surface ozone concentrations in the United States based on model-derived source apportionment

Allen S. Lefohn [a,*], Christopher Emery [b], Douglas Shadwick [c], Heini Wernli [d], Jeagun Jung [b], Samuel J. Oltmans [e]

[a] A.S.L. & Associates, 302 North Last Chance Gulch, Helena, MT 59601, USA
[b] ENVIRON International Corporation, 773 San Marin Drive, Suite 2115, Novato, CA 94945, USA
[c] 320 Eastwood Road, Chapel Hill, NC 27514, USA
[d] Institute for Atmospheric and Climate Science, ETH Zurich, Universitätstrasse 16, 8092 Zurich, Switzerland
[e] CIRES, University of Colorado, NOAA ESRL, Global Monitoring Division, 325 Broadway, Boulder, CO 80305, USA

HIGHLIGHTS

- We present a new approach for characterizing background O_3.
- Highest background occurs during the spring and tends to be related to STT-S.
- Background contributes significantly to total O_3 during non-summer months.
- At urban sites background contributes significantly to mid-range concentrations.

ARTICLE INFO

Article history:
Received 20 August 2013
Received in revised form
25 October 2013
Accepted 14 November 2013

Keywords:
Background ozone
CAMx
Emissions-Influenced Background
Photochemical modeling
Source apportionment
Stratosphere-to-troposphere transport
Surface ozone
Trajectory modeling

ABSTRACT

We analyze background surface ozone (O_3) concentrations as estimated by coupled GEOS-Chem/CAMx models for 23 monitoring sites across the US at high- and low-elevation, rural and urban locations during 2006. Specifically, we consider hourly contributions from global tropospheric O_3 entering North America, stratospheric O_3 over North America, and natural O_3 formed from continental biogenic, fire, and lightning sources according to CAMx source apportionment calculations. Unlike historical modeled background definitions that reflect the absence of anthropogenic emissions, we define "Emissions-Influenced Background" (EIB), which includes chemical interactions with anthropogenic emissions and thus reflects "current" background levels at the sites analyzed. We further define global background O_3 (GBO_3) as the sum of the global tropospheric and stratospheric components and find that higher modeled GBO_3 occurs during the spring at sites across the US. At many of the sites during the spring, fall, and winter months higher GBO_3 is associated with more frequent stratosphere-to-troposphere transport to the surface (STT-S) events according to independent three-dimensional trajectories based on global meteorological analyses. Patterns of higher spring EIB O_3 are followed by lower values during the summer, due to heightened chemical interaction with anthropogenic sources, which are then followed by rising EIB O_3 during the fall and winter months. For some high-elevation western US sites, this seasonal pattern is less discernible due to relatively small anthropogenic contributions and the high EIB O_3 estimated throughout the year. EIB O_3 at all high-elevation sites contributes a significant proportion to total O_3 throughout the year and throughout the observed total O_3 frequency distribution, while EIB O_3 at most urban sites contributes a major portion to total O_3 during non-summer months and to the mid-range concentrations (30–50 ppb) of the frequency distribution.

1. Introduction

While background ozone (O_3) cannot be measured directly, estimating it accurately is important. Background approximations directly affect estimated human health risk and policy expectations regarding emission reduction effectiveness. McDonald-Buller et al.

* Corresponding author. Tel.: +1 406 443 3389.
E-mail addresses: alefohn@asl-associates.com, allen.lefohn@gmail.com (A. S. Lefohn), cemery@environcorp.com (C. Emery), dougshadwick@nc.rr.com (D. Shadwick), heini.wernli@env.ethz.ch (H. Wernli), jjung@environcorp.com (J. Jung), Samuel.J.Oltmans@noaa.gov (S.J. Oltmans).

1352-2310/$ – see front matter © 2013 Elsevier Ltd. All rights reserved.
http://dx.doi.org/10.1016/j.atmosenv.2013.11.033

(2011) and the US Environmental Protection Agency (EPA, 2013) provide a summary of the concepts associated with background O_3 and its relevance to US air quality. Prior to 2006, O_3 measurements from remote monitoring sites were used to estimate background. EPA (1996) estimated hourly average summer background concentrations of 30–50 ppb and applied a background of 40 ppb in its risk analyses. EPA (2006) cited the work of Fiore et al. (2002, 2003), who applied the GEOS-Chem global model to estimate a mean background concentration range of 15–35 ppb. At that time, EPA (2006) defined North American background (NAB) O_3 to include contributions from global anthropogenic and natural sources in the absence of North American (i.e., U.S., Canada, Mexico) anthropogenic emissions. More recently, EPA (2013) has defined US background (USB) O_3 concentrations to include anthropogenic contributions from Canada and Mexico. Modeling results reported by EPA (2013) indicate USB and NAB concentrations tend to be higher in the West (particularly in the Intermountain West) and in the Southwest compared to the East in both spring and summer.

Background O_3 over North America has been recently estimated using the GEOS-Chem global model (Wang et al., 2009; Zhang et al., 2011), the EPA Community Multi-scale Air Quality (CMAQ) regional model (Mueller and Mallard, 2011), the regional Comprehensive Air quality Model with extensions (CAMx; Emery et al., 2012), and the AM3 global model (Lin et al., 2012). Each of these efforts have reported incremental improvements, especially for the higher concentration ranges, by using greater resolution, updated modeling systems, and improved emissions and meteorological datasets. The latest modeling results (Zhang et al., 2011; Emery et al., 2012; Lin et al., 2012) estimate background O_3 ranges of 25–50 ppb across the US, with the highest peaks reaching well over 60 ppb in areas affected by stratospheric intrusion and wildfires in the elevated areas of the western US. For the western US, results from Lin et al. (2012) illustrated the relative importance of stratospheric contributions to NAB.

Recent literature suggests that the stratosphere is a potentially important contributor to background O_3 at high- and low-elevation US monitoring sites (Ambrose et al., 2011; Cooper et al., 2011; Lefohn et al., 2011, 2012; Emery et al., 2012; Langford et al., 2012; Lin et al., 2012). Ambrose et al. (2011) reported that STE and long-range transport affects lower tropospheric O_3 concentrations at the Mt. Bachelor Observatory (2763 m) in central Oregon. Cooper et al. (2011) indicated that descending stratospheric intrusions and Asian pollution plumes influence O_3 concentrations along the California coast. Using trajectory analyses, Lefohn et al. (2011, 2012) reported that stratosphere-to-troposphere transport to the surface (STT-S) frequently coincides with "enhanced" surface O_3 concentrations ($\geq$50 ppb) at both high- and low-elevation monitoring sites across the US during specific months. While STT-S coincidences occur most frequently at high-elevation sites in the western and eastern US during spring, they also noted that coincidences occur at times during the summer, fall, and late winter. Applying the AM3 global chemical transport model, Lin et al. (2012) noted that STT-S during the spring and early summer contributes to surface O_3 concentrations over the western US. Previous literature over the years complement the most recent results cited above concerning the influences of the stratosphere on lower-tropospheric O_3 concentrations (e.g., Reed, 1955; Junge, 1962; Danielsen, 1968; Danielsen, 1975; Danielsen and Mohnen, 1977; Ludwig et al., 1977; Shapiro, 1980; Haagenson et al., 1981; Davies and Schuepbach, 1994; Lamarque and Hess, 1994; Schuepbach et al., 1999; Stohl et al., 2000; Lefohn et al., 2001; Cooper et al., 2005; Cristofanelli et al., 2006; Hocking et al., 2007; Ordóñez et al., 2007; Oltmans et al., 2008; Langford et al., 2009; Akriditis et al., 2010; Cristofanelli et al., 2010).

The purpose of this study is to estimate the hourly or daily background O_3 contributions to total O_3 throughout 2006 at 16 urban and 7 rural monitoring sites across the US and to explore reasons for the range of uncertainties associated with these estimates. Coupled global (GEOS-Chem) and regional (CAMx) photochemical transport modeling (Emery et al., 2012) is used to estimate 2006 global tropospheric, stratospheric, and North American natural contributions to hourly background O_3 concentrations over the US. STT-S estimates derived from Lagrangian Analysis Tool (LAGRANTO) trajectory calculations (Lefohn et al., 2012) are used to investigate relationships between simulated background contributions and observed O_3, and to characterize the seasons and locations where stratospheric and upper tropospheric O_3 contributes to elevated surface O_3 at 23 monitoring locations.

Uniquely, this study defines a new metric that we refer to as "Emissions-Influenced Background" (EIB) O_3. EIB is apportioned to global tropospheric O_3 and stratospheric O_3 entering North America (collectively referred to as Global Background O_3 or GBO_3) and natural O_3, formed in North America from continental biogenic, fire, and lightning sources. The simulation of all three EIB components includes chemical decay via interactions with North American anthropogenic and natural precursor emissions of nitrogen oxides (NO_x), volatile organic compounds (VOC), and carbon monoxide (CO). Unlike historical modeled background definitions that reflect the absence of anthropogenic emissions (thus maximizing O_3 lifetime), we define EIB to include chemical interactions with anthropogenic emissions; thus reducing O_3 lifetime in the polluted boundary layer and reflecting "current" background levels at the sites analyzed. In pristine areas with small anthropogenic influences, EIB is similar to NAB. In urban areas EIB is chemically decayed but it converges upward toward the higher NAB metric as anthropogenic emissions are reduced.

EIB O_3 estimates are subject to systematic and unsystematic model errors that vary site-to-site. Our methodology estimates the hourly range of EIB uncertainty associated with site-specific error in total O_3 by distributing that error to global and natural/anthropogenic components. The upper uncertainty range serves as a lower bound estimate for USB. Monthly and seasonal patterns of STT-S frequency are used to explore possible reasons for some of these uncertainties.

2. Approach

2.1. Selection of surface ozone monitoring sites

Measured hourly 2006 O_3 data at 23 US monitoring sites were downloaded from the EPA Air Quality System (AQS) and Clean Air Status and Trends Network (CASTNet). The 23 monitoring sites represent high/low elevation, urban/rural environments, and east/central/west geography across the US (Fig. 1; Table 1). Sixteen urban monitoring sites were analyzed in this study, one from each city addressed in the EPA's human health risk analyses (US EPA, 2012). Usually, the selected site reported the highest 3-year average of the 4th highest daily maximum 8-h average concentration over 2006–2008 (consistent with the US O_3 standard). In some cases we selected a site reporting a similar peak but more representative of the city-wide population distribution. The remaining 7 sites were singularly located in rural environments and had been previously characterized by Lefohn et al. (2012). All rural and most urban sites collected data over a 12-month period although seven of the urban sites had shorter monitoring seasons (Table 1). The 2006 data capture averaged 95% over the 23 sites.

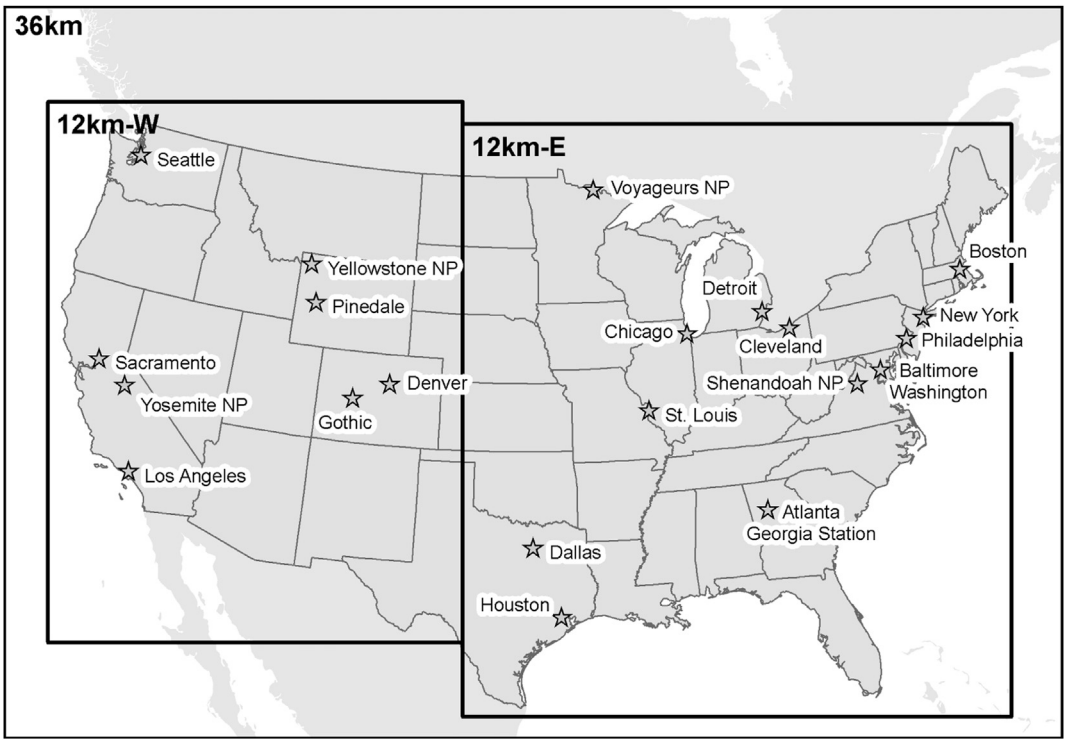

Fig. 1. Depiction of the CAMx 36 km modeling grid (full extent of figure), and 12 km western and eastern US modeling grids (insets).

2.2. Description of the model system

2.2.1. Global modeling

The GEOS-Chem global model, version 8-03-01 (Harvard, 2013), was used to derive boundary condition inputs for regional modeling following the approach of Emery et al. (2012). GEOS-Chem was run for 2006 on a 2° × 2.5° latitude/longitude grid with 47 vertical layers, using 3-h surface and 6-h aloft GEOS-5 global meteorological analyses (GMAO, 2013). Standard and default settings, solvers, algorithms, and datasets were used to treat emissions, chemistry, transport, and removal. Gases and aerosols were resolved with 43 chemical species, and the "LINOZ" stratospheric O_3 treatment was employed. NO_x emissions in Japan and Korea were increased two-fold relative to the 2006 inventory for Asia (Zhang et al., 2011; Emery et al., 2012).

2.2.2. Regional modeling

The Comprehensive Air quality Model with extensions (CAMx), version 5.40 (ENVIRON, 2011) was run following the approach of Emery et al. (2012) for 2006 on a nested grid system covering the North American continent (Fig. 1). All three grids possessed identical 34 vertical layer structures spanning the entire troposphere and lower stratosphere up to a pressure altitude of 50 hPa (~20 km). Gas-phase photochemistry was treated with the Carbon Bond 2005 mechanism (CB05; Yarwood et al., 2005), ignoring particulate matter (PM). Standard and default transport, diffusion and removal algorithms were employed. Chemical boundary conditions for the outer CAMx grid were defined from 3-h GEOS-Chem concentration output fields mapped to the CAMx CB05 compounds.

The EPA (2006) meteorological and emission datasets used were derived as part of the Air Quality Model Evaluation International Initiative (AQMEII) program (Rao et al., 2011; Vautard et al., 2012; Pouliot et al., 2012). Surface snow-cover fields were improved from those employed by Emery et al. (2012), which reduced deposition rates and mitigated winter and early spring O_3 underprediction over much of the US. Emery et al. (2012) augmented AQMEII emission estimates with updated 2005/2006 emission inventories for the western US oil and gas development sector, and with lightning NO_x emission estimates following the approach of Koo et al. (2010).

CAMx was run with the Ozone Source Apportionment Tool (OSAT; Dunker et al., 2002) to track contributions to hourly O_3 throughout the entire nested grid system from the following sources:

- All natural continental sources of NO_x and VOC (biogenic, fires, lightning NO_x) within the North American modeling domain;
- Ozone entering the domain above 10 km altitude (a marker for stratospheric O_3);
- Ozone entering the domain below 10 km (a marker for global tropospheric O_3).

In the Discussion and Conclusion section, we discuss issues in selecting the 10 km criterion.

Since North American emissions were not removed from the global model, the global tropospheric O_3 component includes dilute contributions from North American emissions that have traveled around the world. Our definition of fires include all large events prepared in the AQMEII inventory (Pouliot et al., 2012), including wildfires, prescribed and agricultural burning. North American anthropogenic contributions within the modeling domain were determined by subtracting the contributions listed above from the simulated total O_3. OSAT preferentially allocates O_3 formed from interactions between anthropogenic NO_x and natural VOC to the controllable anthropogenic sector. Therefore, OSAT limits the portion of background O_3 allocated to natural precursors to interactions between natural NO_x and VOC, an explicit design objective of the EIB calculation.

Table 1
O_3 monitoring sites used in the study.

Site Name	Site ID	LU[a]	Latitude	Longitude	Elevation (m)	Months
Atlanta, GA	132470001	RA	33°35′ N	84°04′ W	219	March–October
Baltimore, MD	240053001	SR	39°18‘ N	76°28‘ W	5	January–December
Boston, MA	250092006	UC	42°28‘ N	70°58‘ W	52	January–December
Chicago, IL	170310001	SR	41°40‘ N	87°43‘ W	188	January–October
Cleveland, OH	390355002	SR	41°32‘ N	81°27‘ W	328	April–October
Dallas, TX	481130087	SC	32°40‘ N	96°52‘ W	205	January–December
Denver, CO	080590006	RI	39°54‘ N	105°11′ W	1802	January–December
Detroit, MI	261630019	SR	42°26‘ N	83°00‘ W	192	April–September
Georgia Station, GA	GAS153	RA	33°10‘ N	84°24′ W	270	January–December
Gothic, CO	GTH161	R	38°57′ N	106°59′ W	2926	January–December
Houston, TX	482010055	UR	29°42‘ N	95°30‘ W	18	January–December
Los Angeles, CA	060719004	SC	34°06‘ N	117°16‘ W	318	January–December
New York, NY	361030004	RA	40°57‘ N	72°43‘ W	31	April–October
Philadelphia, PA	420170012	SR	40°06‘ N	74°53‘ W	12	April–October
Pinedale, WY	PND165	RF	42°55‘ N	109°47′ W	2388	January–December
Sacramento, CA	060670012	SR	38°41′ N	121°09′ W	98	January–December
Seattle, WA	530330023	RF	47°08‘ N	121°55‘ W	402	May–September
Shenandoah NP, VA	511130003	RF	38°31‘ N	78°26′ W	1073	January–December
St. Louis, MO	291831002	RA	38°52‘ N	90°13‘ W	131	April–October
Voyageurs NP, MN	271370034	RF	48°24‘ N	92°49′ W	429	January–December
Washington DC	110010043	UC	38°55‘ N	77°01‘ W	50	January–December
Yellowstone NP, WY	560391011	RF	44°34‘ N	110°24′ W	2468	January–December
Yosemite NP (Turtleback Dome), CA	060430003	RF	37°42′ N	119°42′ W	1605	January–December

[a] LU, land use; R, rural; RA, rural agricultural; RF, rural forest; RI, rural industrial; SC, suburban commercial; SR, suburban residential; UC, urban commercial; UR, urban residential; NP, national park.

2.3. Identification of stratospheric intrusions

A Lagrangian trajectory method was used to diagnose STT events down to the surface (STT-S) as described by Lefohn et al. (2012). The trajectory model of Wernli and Davies (1997) was used to identify STT events following the method discussed by Wernli and Bourqui (2002) for compiling multi-year climatologies of such events. Specifically, we identified days when STT-S trajectories coincided with enhanced surface O_3 at specific monitoring sites. The model provided trajectory coordinate information every 6 h. Once a trajectory came close to the surface using the criteria discussed below, we regarded the subsequent 18 h as potentially relevant for impacting surface O_3 concentrations.

Our method consisted of the following specific steps:

1. Every day at 00 UTC, 24-h forward trajectories were initiated from a regular grid around the extratropical tropopause in the Northern Hemisphere. A horizontal resolution of 80 km and a vertical resolution of 30 hPa (between 80 and 590 hPa) ensured that every trajectory represented a consistent initial mass of air. From this large set of 24-h trajectories, only those that crossed the tropopause from above were retained. The tropopause pressure was defined at every grid point as the higher pressure value of the 380-K and the 2-pvu isentropes. An initial potential vorticity value larger than 2 pvu was a prerequisite for considering trajectories that were associated with stratospheric O_3 values.
2. The retained trajectories were extended four days backward and ten days forward in time; a one-day residence-time threshold (Wernli and Bourqui, 2002) was used to select “potentially significant” exchange trajectories.
3. From the identified stratospheric intrusions, represented by 10-day forward trajectories from the point of tropopause intersection, the intrusions penetrating close to the surface, i.e., with an isentropic difference between the air parcel and the surface ($\Delta\theta$) of less than 5 K, were selected as STT-S trajectories. Lefohn et al. (2011, 2012) discuss the rationale for the 10-day forward trajectory criterion.

2.4. Global background and STT-S analyses

We used a conditional qualitative analysis approach in this study because of the continuous concentration variability related to STT strength, dispersion processes, and chemical decay during descent (Lefohn et al., 2012). We combined diagnosed STT-S events from trajectory modeling with model-derived source apportionment estimates to identify when transport from the stratosphere and upper troposphere enhanced simulated background O_3 at the surface. We tabulated those months showing a relationship between higher global background concentrations and STT-S events.

Hourly modeled GBO_3 was constructed from hourly CAMx source apportionment estimates of global tropospheric and stratospheric O_3 components at each of the 23 sites listed in Table 1:

$$\text{Modeled } GBO_3 = \text{Global Tropospheric } O_3 + \text{Stratospheric } O_3. \quad (1)$$

An alternative estimate for GBO_3 was also determined from hourly observed total O_3 by subtracting off hourly modeled anthropogenic and continental natural O_3 components:

$$\text{Alternative } GBO_3 = \text{Observed Total } O_3 - \text{Anthropogenic } O_3 - \text{Natural } O_3. \quad (2)$$

According to the amount of hourly error associated with modeled GBO_3 and anthropogenic plus natural components, the alternative GBO_3 concentration can be greater than, equal to, or less than the modeled GBO_3 concentration. As we describe more extensively below, comparisons of modeled and alternative GBO_3 is a unique technique developed specifically for this analysis to provide clues into whether GBO_3 or the anthropogenic component were the primary sources of seasonal model error. The more typical comparison between modeled total O_3 to observed total O_3 is not optimum for providing indications as to which contributing component dominates the error.

A set of conditional analyses was performed combining results from the GEOS-Chem/CAMx model and LAGRANTO trajectories. The analyses provided information describing the relationship between diagnosed STT-S events and maximum daily 8-h average (MDA8) GBO_3 concentrations. The steps undertaken in the study for each of the 23 sites were as follows:

1. Identify months when paired (day and site) modeled and alternative MDA8 GBO_3 concentrations were high;
2. Identify months when MDA8 GBO_3 concentrations above the monthly median were coincident with STT-S events;
3. Overlay Steps 1 with 2 to identify months when (1) the highest MDA8 GBO_3 occurred and (2) diagnosed STT-S events coincided with the highest MDA8 GBO_3 during the month;
4. Identify months exhibiting under and over predictions of modeled total O_3; and
5. Combine Steps 3 and 4 to suggest evidence whether model uncertainty was associated with GBO_3 or anthropogenic plus natural O_3.

In Step 5, we collectively refer to the anthropogenic plus natural O_3 components as "anthropogenic" because generally the natural component was relatively small and local chemical interactions between the two were mostly assigned to the anthropogenic component by the OSAT technique.

2.5. Estimating EIB uncertainty

Model estimates of EIB O_3 include global tropospheric, stratospheric, and natural components. Each are subject to model errors that vary site-to-site. From a chemical standpoint, model uncertainties at the local scale include biases in the relative abundance of NO_x to form and titrate O_3, which is often under predicted because coarse resolution artificially dilutes emissions, but which can be over predicted when ventilation processes, such as vertical mixing are inappropriately suppressed. An over-abundance of VOCs can lead to both excessive local O_3 production and excessive chemical removal of background O_3. These specific issues differ from the broader background modeling uncertainties outlined by Emery et al. (2012) such as errors in global emission estimates, resolution- and algorithm-related uncertainties in both global and regional models, and gross approximations for background sources that are difficult to quantify (e.g., fires, lightning, and STT).

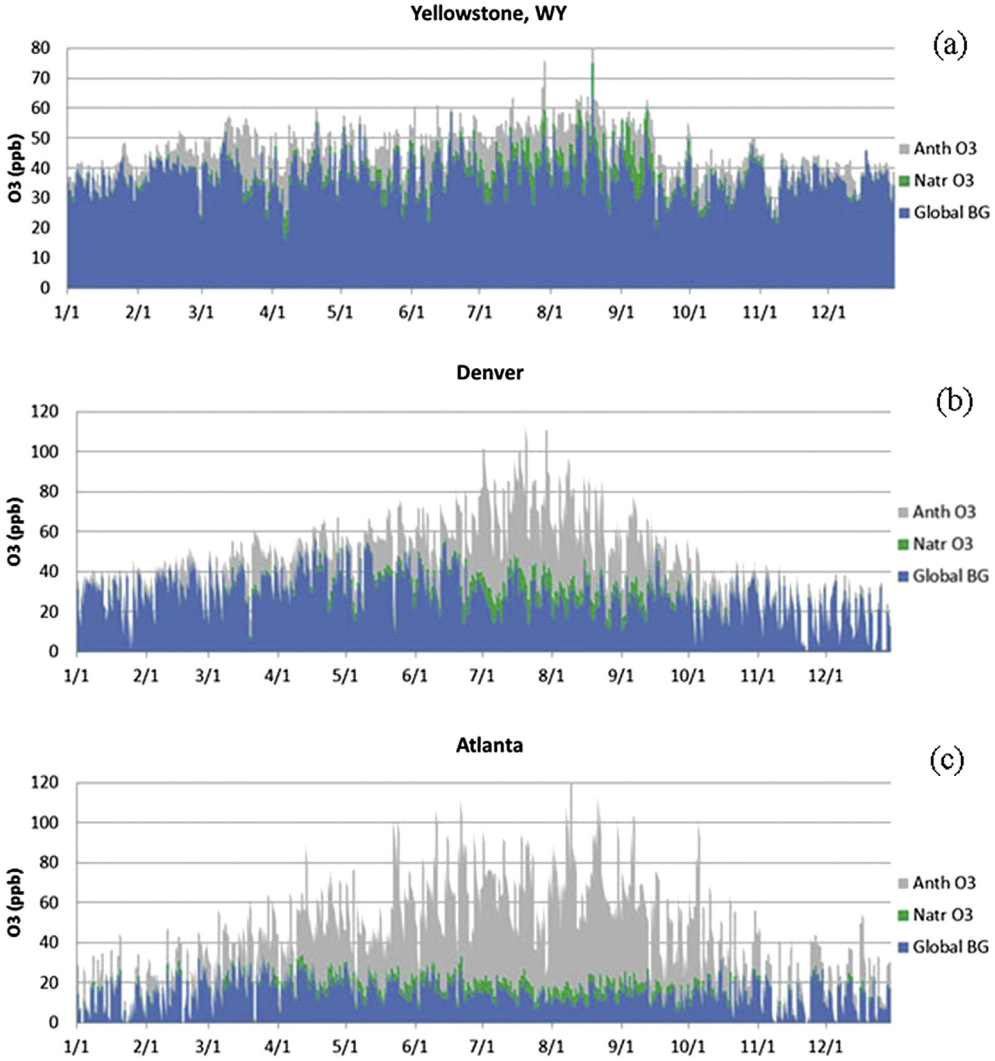

Fig. 2. Modeled contributions of hourly GBO_3 (global tropospheric O_3 plus stratospheric O_3), natural (Natr O_3), and anthropogenic (Anth O_3) adding to total hourly O_3 for a) Yellowstone NP, b) Denver and c) Atlanta.

Our technique to estimate the range of 2006 EIB uncertainty distributes the hourly relative error between paired predicted and observed total O_3 proportionally to the modeled background and anthropogenic components to maintain a consistent background-to-anthropogenic ratio. In the absence of information to allocate error with more accuracy (e.g., clear remote surface impacts from STT), this first-order assumption is considered appropriate. The resulting hourly EIB ranges are specific to the 2006 modeling dataset.

Simulated and observed total O_3 were paired by site and hour. When an hour's simulated total O_3 was lower than observed, all four modeled components (global troposphere, stratosphere, natural, anthropogenic) were scaled up to match the monitored total O_3; the minimum of the hourly EIB range was set to the original (un-scaled) value and the maximum of the hourly range was set to the scaled-up value. In cases of over prediction, all O_3 components were scaled down; the maximum of the hourly EIB range was set to the original (un-scaled) value, and the minimum of the hourly range was set to the scaled-down value. In cases where the un-scaled maximum background was higher than the observed total O_3, the maximum was set equal to the scaled-down minimum and no range was calculated. For hours with missing observations, the minimum and maximum concentrations were set to the original simulated (un-scaled) value.

3. Results

We evaluated CAMx simulated hourly total O_3 against observations at all 23 sites in terms of monthly mean fractional bias (MFB). The MFB metric is a robust and commonly-used statistic for air quality evaluations; it is symmetric around zero bias and ranges between ±200%. MFB is defined as $(2/n)\Sigma[(P_i\text{-}O_i)/(P_i + O_i)]$, where P_i is an hourly prediction, O_i is the site- and time-paired hourly observation, and the sums are taken over all n valid hourly pairs in a month. Monthly MFB for each site's monitoring period is tabulated in the Supplement Appendix (Table S1). These biases are consistent with earlier multi-model studies (e.g., Reidmiller et al., 2009; Zhang et al., 2011; Emery et al., 2012). Generally, the high elevations sites tended toward under prediction, with some sites over predicting during the summer. Model performance at low-elevation sites tended toward larger under prediction biases in cool months (November–April) and larger over prediction biases in warm months (June–October), particularly for sites in the southern and eastern US.

In presenting source apportionment analyses for all 23 sites, we focus on graphical results for three example sites (Yellowstone National Park, Denver, and Atlanta) that represent very different climate and emission environments. Graphics for the remaining 20 sites are presented in the Supplement Appendix. Fig. 2 displays the hourly modeled O_3 source apportionment contributions (adding to

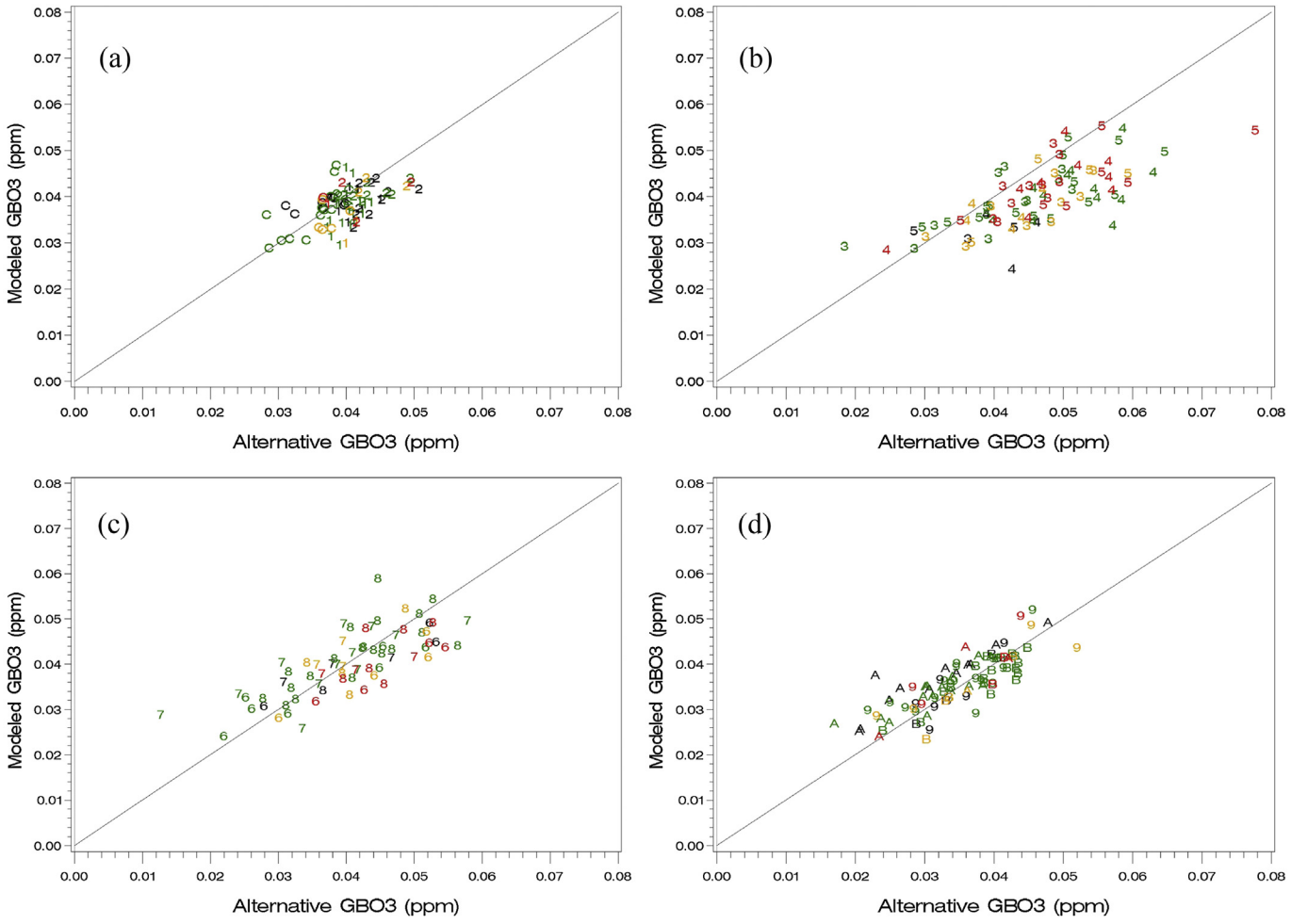

Fig. 3. Scatter plots of MDA8 concentrations of modeled GBO_3 vs. alternative GBO_3 for the Yellowstone NP, Wyoming for (a) winter, (b) spring, (c) summer, and (d) fall. Each datum is labeled for month (1–9 = January–September; A-C = October–December); the coinciding daily STT-S "hits" are color-indicated (black = 0, green = 1–10, orange = 11–20, and red ≥ 20).

an hourly total O_3) from the global background, anthropogenic, and natural components during 2006 at these sites (see Fig. S1 for remaining sites). The western rural high-elevation site at Yellowstone National Park (NP) was dominated by GBO_3 throughout the year with minor anthropogenic or continental natural contributions as indicated in Fig. 2a. GBO_3 remained elevated at the western urban high-elevation site in Denver (Fig. 2b), but anthropogenic effects are evident, including episodic NO_x titration of O_3 toward zero throughout the year and heightened O_3 production from local anthropogenic/natural sources during the warm season. GBO_3 was much lower at the eastern urban low-elevation site in Atlanta with local anthropogenic O_3 production and GBO_3 decay much more evident (Fig. 2c). Here GBO_3 contributed larger proportions to total O_3 during the spring, winter, and fall but was lowest during the summer.

Relationships between modeled GBO_3, alternative GBO_3, and diagnosed STT-S events throughout the year were evaluated primarily from scatter diagrams constructed for each of the 23 monitoring sites. These plots compare MDA8 modeled vs. alternative GBO_3, where each daily scatter point is annotated to indicate month and any coincident STT-S events. From the plots, we infer the attribution of under or over predictions to (1) anthropogenic O_3 + natural O_3 or (2) global tropospheric O_3 + stratospheric O_3. Examples are shown by season in Figs. 3–5 for Yellowstone NP, Denver, and Atlanta, where each point is labeled for the specific month in which it occurs (1–9 denote January–September and A–C denote October–December); the number of diagnosed daily STT-S "hits" coinciding with each data point (i.e., STT-S trajectories within 250 km of the monitor location) is color-coded where black = 0, green = 1–10, orange = 11–20, and red ≥ 20.

Our results indicated biases that were site and seasonally related. If the GEOS-Chem/CAMx model perfectly simulated observed total O_3, the values of modeled GBO_3 and alternative GBO_3 would fall on the 1:1 line (see Figs. 3–5). Points below the 1:1 line indicate that O_3 was under predicted and points above indicate that O_3 was over predicted. A vertical line is plotted at zero alternative GBO_3. Negative values of alternative GBO_3 (i.e., observed total O_3 − anthropogenic O_3 − natural O_3) to the left of the vertical line indicate that modeled anthropogenic + natural O_3 component was higher than observed total O_3 and thus mostly the cause of over predictions.

3.1. *Months when modeled and alternative GBO_3 were high*

At most sites, the highest concentrations of modeled and alternative MDA8 GBO_3 occurred during the same months (Table S2). The highest median concentrations for both forms of GBO_3 tended to occur during the late winter (February), spring (March–May), and early summer (June) periods. The western high-elevation sites (Yosemite NP, Denver, Gothic, Pinedale, and

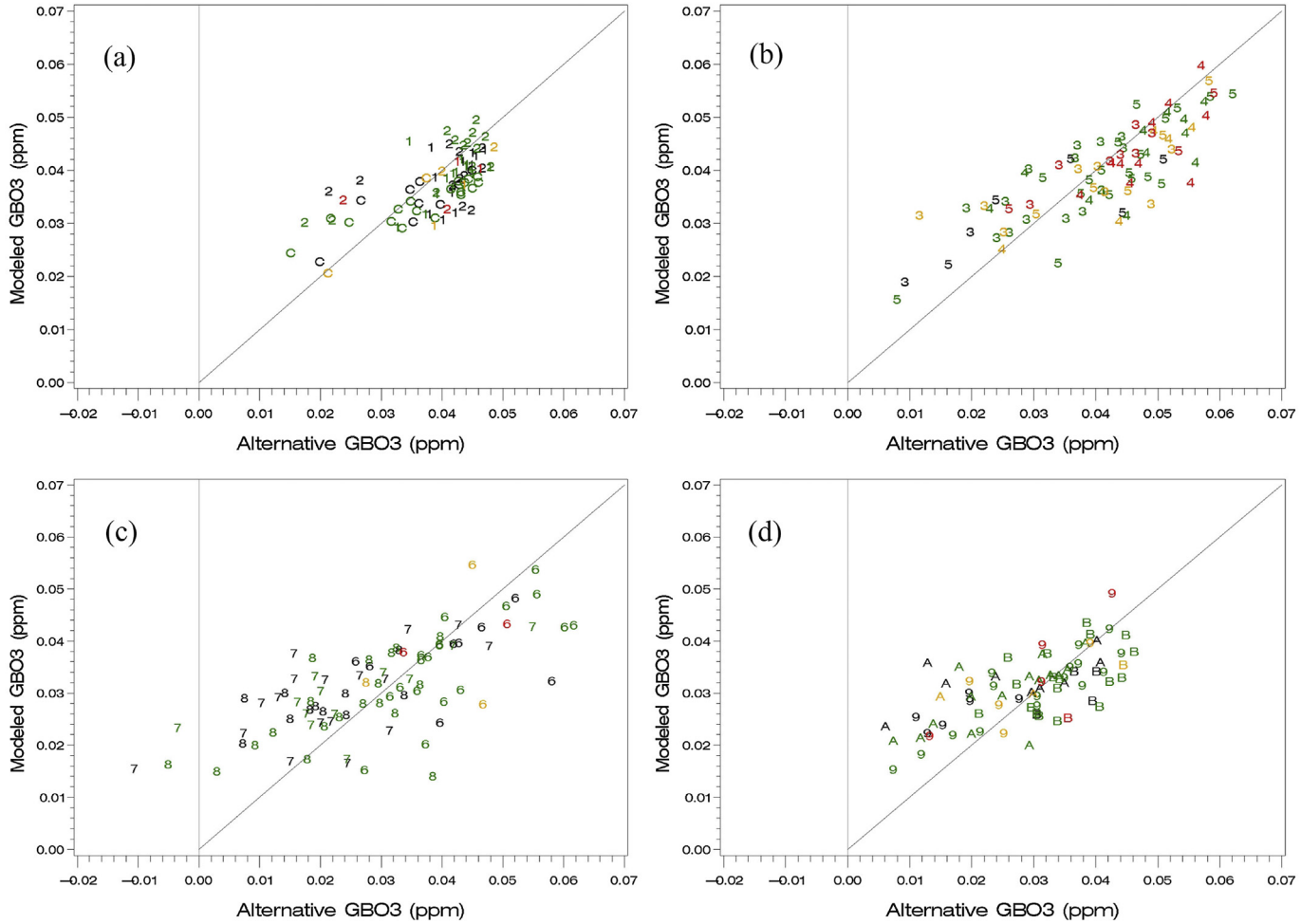

Fig. 4. Scatter plots of MDA8 concentrations of modeled GBO_3 vs. alternative GBO_3 for Denver, Colorado for (a) winter, (b) spring, (c) summer, and (d) fall. Each datum is labeled for month (1–9 = January–September; A-C = October–December); the coinciding daily STT-S "hits" are color-indicated (black = 0, green = 1–10, orange = 11–20, and red ≥ 20).

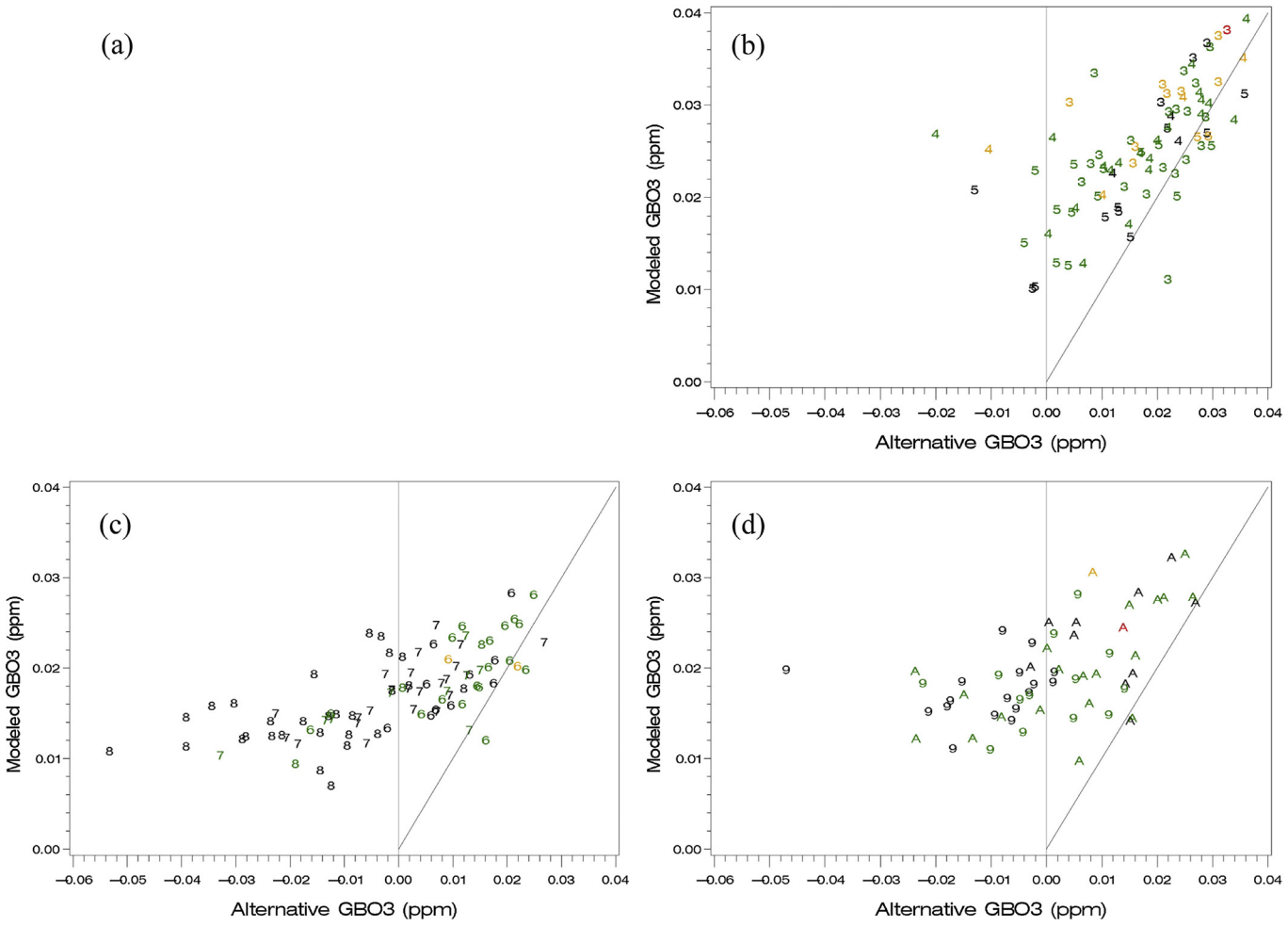

Fig. 5. Scatter plot of MDA8 concentrations of modeled GBO_3 vs. alternative GBO_3 for Atlanta, Georgia for (a) winter (no data), (b) spring, (c) summer, and (d) fall. Each datum is labeled for month (1–9 = January–September; A-C = October–December); the coinciding daily STT-S "hits" are color-indicated (black = 0, green = 1–10, orange = 11–20, and red ≥ 20).

Yellowstone NP) exhibited higher median concentrations over more seasons compared to urban, low-elevation, or eastern settings, where higher median concentrations in late winter and spring predominated.

3.2. Months when above-median GBO_3 was coincident with STT-S events

Figs. 3–5 provide insight concerning the relationship between diagnosed STT-S events and the magnitude of the daily maximum MDA8 GBO_3 concentrations. When evaluating the relationship, the associations infer that some amount of stratospheric O_3 appears to enhance the observed MDA8 GBO_3 concentration and not that MDA8 concentrations are 100% influenced by STT-S. For example, at Yellowstone NP, the diagnosed STT-S events (shown by red, orange, and green symbols in Fig. 3) frequently occurred and were distributed throughout the entire range of daily maximum MDA8 GBO_3 concentrations. Many of the GBO_3 concentrations at Denver were also associated with diagnosed STT-S events (Fig. 4). At Atlanta, the higher GBO_3 concentrations were more often associated with diagnosed STT-S hits, whereas the lower concentrations were not (Fig. 5).

To identify those months exhibiting a relationship between diagnosed STT-S events and high GBO_3, we rank-ordered the monthly MDA8 concentrations, separating the distributions at the median into a top and a bottom half. For each half, the median number of diagnosed STT-S hits was calculated.

Table S3 notes months when MDA8 GBO_3 in the top half coincided with a greater number of daily diagnosed STT-S hits than the bottom half. The high-elevation sites had higher GBO_3 coinciding with greater numbers of daily diagnosed STT-S hits compared to the lower concentrations, but frequent instances when diagnosed STT-S hits occurred over the entire month. For high-elevation sites, the asterisk symbol (*) in Table S3 indicates months when diagnosed STT-S hits occurred over the entire distribution of GBO_3, a characteristic of almost every high-elevation site (western and eastern US) and for nearly all months. At lower-elevation sites, the higher GBO_3 concentrations were associated with a greater number of diagnosed STT-S events during winter, spring, early summer (June), and fall (September and October).

3.3. Months when STT-S events coincided with months of highest GBO_3

Overlaying Tables S2 and S3 identified months when (1) the highest MDA8 GBO_3 occurred (Table S2) and (2) more diagnosed STT-S events coincided with above-median MDA8 GBO_3 than below-median GBO_3 (Table S3). Table 2 illustrates that these coincidences tended to occur more often in western and eastern high-elevation sites during the late winter (February), spring, and early

Table 2
Months when MDA8 GBO_3 was high, and above-median MDA8 GBO_3 coincided with a larger number of daily STT-S events compared to below-median GBO_3.

Site Name	Jan	Feb	Ma	Apr	May	June	July	Aug	Sept	Oct	Nov	Dec
High Elevation												
Yosemite NP, CA	x	x	x	x	x	x		x		x		
Denver, CO	x	x	x	x	x	x						
Gothic, CO	x	x	x	x	x	x						
Pinedale, WY		x	x	x	x							
Yellowstone NP, WY		x	x	x	x	x	x	x				
Shenandoah NP, VA		x	x	x								
Low Elevation												
Atlanta, GA			x	x								
Baltimore, MD			x									
Boston, MA		x										
Chicago, IL		x										
Cleveland, OH				x								
Dallas, TX			x									
Detroit, MI					x							
Georgia Station, GA				x								
Houston, TX			x									
Los Angeles, CA		x		x	x	x						
New York, NY				x								
Philadelphia, PA					x							
Sacramento, CA		x		x	x							
Seattle, WA												
St. Louis, MO				x	x					x		
Voyageurs NP, MN					x							
Washington DC			x									

summer (June) months. Urban low-elevation urban sites exhibited such patterns only during spring (March–May).

3.4. Tabulating months by under and over predictions

As described earlier in this section, we explored relationships between modeled and alternative MDA8 GBO_3 (Figs. 3–5) by tabulating monthly model under- or over-prediction tendencies. For example, the scatter of daily MDA8 concentrations for Yellowstone NP (Fig. 3) were centered evenly above and below the 1:1 line and indicated a relatively small proportion of model error. The scatter for Denver (Fig. 4) also appeared evenly distributed, but more widely (model error) and with a few points to the left of the vertical zero line. Most of the Atlanta points (Fig. 5) were above the 1:1 line with many points in July, August and September extending to the left of the vertical zero line. Negative values of alternative MDA8 GBO_3 to the left of the vertical zero line indicate that modeled anthropogenic O_3 alone was higher than observed total O_3 and thus mostly the cause of over predictions.

To identify monthly relationships between modeled and alternative MDA8 GBO_3, we calculated the ratio of their medians. The ratio is a simple indicator of under and over prediction and should not be used to infer an absolute amount of uncertainty. A monthly ratio less (greater) than 1 indicates GBO_3 and/or anthropogenic O_3

Table 3
Ratio of median modeled MDA8 GBO_3 to median alternative MDA8 GBO_3 by month. The asterisk (*) indicates that the alternative GBO_3 median concentration was low and the resulting ratio was very large.

Site name	Jan	Feb	Mar	Apr	May	June	July	Aug	Sept	Oct	Nov	Dec
West and Intermountain West												
Yosemite NP, CA	1.02	1.08	0.85	0.86	0.81	0.91	0.91	0.77	0.76	0.91	1.19	1.07
Denver, CO	0.94	0.94	0.98	0.87	0.86	0.93	1.40	1.22	1.17	1.13	0.93	0.95
Gothic, CO	0.97	1.01	0.91	0.90	1.00	1.10	1.40	1.23	1.16	1.05	1.00	0.98
Pinedale, WY	0.90	0.93	0.96	0.93	0.87	**	1.07	1.04	1.03	1.07	1.02	1.00
Yellowstone NP, WY	0.92	0.95	0.88	0.87	0.81	0.95	1.01	1.00	1.06	1.08	0.95	1.03
Shenandoah NP, VA	0.91	1.10	1.05	0.85	1.02	0.98	1.86	1.25	1.67	1.17	1.00	0.92
Lower Elevation												
Atlanta, GA			1.33	1.43	1.72	1.42	6.26	−1.13	−3.64	2.47		
Baltmore, MD	1.22	1.25	1.11	1.22	1.26	2.17	−6.46	2.41	2.86	1.85	1.42	1.08
Boston, MA	0.89	0.99	0.89	0.97	0.88	2.48	*	1.86	1.55	1.12	1.01	0.89
Chicago, IL	1.12	1.18	1.37	1.17	1.43	1.42	*	2.80	1.72	1.16		
Cleveland, OH				1.05	0.99	1.12	3.22	1.84	1.32	0.86		
Dallas, TX	0.89	0.89	0.90	0.99	0.93	0.86	1.83	1.56	0.80	1.06	1.05	0.98
Detroit, MI				0.86	0.71	0.96	1.34	1.53	1.00			
Georgia Station, GA	0.98	1.17	1.05	1.05	1.04	0.98	1.69	*	6.46	1.75	1.42	1.17
Houston, TX	0.97	0.96	1.15	1.24	1.15	1.70	−7.14	7.08	1.20	0.90	1.10	1.05
Los Angeles, CA	1.18	1.09	0.96	1.06	0.73	0.80	3.04	0.92	1.03	0.88	1.07	1.18
New York, NY				0.99	0.88	1.34	−4.09	2.59	2.96	1.37		
Philadelphia, PA				1.05	1.01	1.67	*	2.55	3.18	1.44		
Sacramento, CA	0.95	1.15	0.94	0.98	0.99	1.09	1.14	1.02	1.06	0.93	1.12	1.32
Seattle, WA					0.85	1.01	1.12	1.39	1.49			
St. Louis, MO				0.91	1.15	1.15	1.51	3.92	1.78	1.15		
Voyageurs NP, MN	0.88	0.88	0.84	0.80	0.85	0.97	1.16	1.10	0.81	0.97	1.03	0.90
Washington DC	0.78	1.28	1.08	1.17	1.04	1.13	*	1.43	1.78	1.71	2.09	0.67

**Poor data capture in June for Pinedale.

Table 4
Months when STT-S events coincided with months of the highest MDA8 GBO_3 and the model tended to be under (u) or over (o) predicted.

Site Name	Jan	Feb	Mar	Apr	May	June	July	Aug	Sept	Oct	Nov	Dec
High Elevation												
Yosemite NP, CA	o	o	u	u	u	u		u		u		
Denver, CO	u	u	u	u	u	u						
Gothic, CO	u	o	u	u	o	o						
Pinedale, WY		u	u	u	u							
Yellowstone NP, WY		u	u	u	u	u	o	o				
Shenandoah NP, VA		o	o	u								
Low Elevation												
Atlanta, GA			o	o								
Baltimore, MD			o									
Boston, MA		u										
Chicago, IL		o										
Cleveland, OH				o								
Dallas, TX			u									
Detroit, MI					u							
Georgia Station, GA				o								
Houston, TX			o									
Los Angeles, CA		o		o	u	u						
New York, NY				u								
Philadelphia, PA					o							
Sacramento, CA		o		u	u							
Seattle, WA												
St. Louis, MO				u	o					o		
Voyageurs NP, MN					u							
Washington DC			o									

under predictions (over predictions). A negative ratio indicates generally that anthropogenic O_3 was over predicted (left of the vertical alternative GBO_3 line). The ratio between median MDA8 modeled and alternative GBO_3 by month is summarized in Table 3. In almost all cases, western US (Yosemite NP, Denver, Gothic, Pinedale, and Yellowstone NP) high-elevation sites exhibited median ratios < 1 (under predictions) during the spring (March–May). Many low-elevation sites (Boston, Dallas, Detroit, Los Angeles, New York, Sacramento, Seattle, St. Louis, and Voyageurs NP) also indicated such spring under predictions. At several eastern sites (Atlanta, Baltimore, Chicago, Georgia Station, Houston, Philadelphia, Shenandoah NP, and Washington DC), over predictions occurred during many months, especially July–October. Given the small decayed levels of warm-season GBO_3 at these sites, it is likely that these over predictions were associated with anthropogenic O_3. For example, Atlanta, Baltimore, Chicago, Houston, and New York

Table 5
Fraction (%) of days when STT-S > 0 and MDA8 GBO_3 was below the 1:1 line (left monthly value), and fraction of days when STT-S $= 0$ and the MDA8 GBO_3 was above the 1:1 line (right monthly value). The **blue** numbers identify the specific months when STT-S was associated with GBO_3 below the 1:1 line. The **red** numbers identify the specific months when STT-S was not associated with GBO_3 above the 1:1 line.

Site Name	Jan	Feb	Mar	Apr	May	June	July	Aug	Sept	Oct	Nov	Dec
High Elevation												
Yosemite NP, CA	73/16	89/68	100/0	96/0	83/0	81/22	63/42	90/0	75/0	85/0	100/22	86/17
Denver, CO	67/67	47/31	100/11	100/0	91/33	76/20	57/63	83/44	100/29	56/26	72/0	77/50
Gothic, CO	75/20	47/15	100/0	93/0	*	92/6	25/41	100/27	100/20	86/29	*	67/14
Pinedale, WY	75/50	57/14	100/0	91/0	90/27	**	85/11	100/10	91/16	88/30	93/6	*
Yellowstone NP, WY	82/50	52/14	96/0	89/0	96/25	89/25	83/16	*	70/10	100/50	90/11	83/33
Shenandoah NP, VA	50/50	50/28	93/6	91/25	89/31	67/33	43/58	100/48	100/52	67/24	*	90/57
Low Elevation												
Atlanta, GA			100/12	100/11	67/38	100/37	0/70	0/90	0/60	50/30		
Baltimore, MD	69/65	50/40	100/22	83/21	100/39	75/58	0/68	50/66	100/67	50/48	63/55	90/45
Boston, MA	43/43	62/60	77/20	95/36	29/50	29/78	33/54	60/69	33/42	36/55	38/53	76/20
Chicago, IL	20/75	50/54	69/44	90/25	78/59	67/42	75/70	67/54	75/73	57/28		
Cleveland, OH				70/16	71/41	45/58	0/62	0/69	43/78	64/56		
Dallas, TX	55/20	27/54	72/31	85/41	53/88	57/67	63/83	75/85	57/56	53/44	40/67	57/44
Detroit, MI				83/14	74/50	71/44	45/60	50/65	*			
Georgia Station, GA	45/70	43/43	90/14	77/6	58/32	79/44	20/62	0/90	100/69	50/24	67/37	75/36
Houston, TX	47/27	36/82	100/58	40/60	50/88	14/81	0/100	50/97	50/83	20/56	25/67	69/47
Los Angeles, CA	70/35	75/55	86/0	92/13	60/55	59/50	14/96	38/40	44/57	81/27	60/33	100/25
New York, NY				75/36	25/47	14/100	0/79	50/76	100/44	80/50		
Philadelphia, PA				91/6	83/33	63/50	0/68	0/65	67/52	43/40		
Sacramento, CA	43/44	36/59	78/8	77/41	85/18	79/63	55/55	62/44	50/61	71/57	75/56	71/48
Seattle, WA					76/8	64/31	45/60	63/43	56/45			
St. Louis, MO				86/13	67/58	100/35	17/52	0/59	67/52	67/35		
Voyageurs NP, MN	20/80	29/0	54/43	88/0	64/33	67/25	78/33	67/13	56/25	58/75	23/59	36/75
Washington DC	56/58	33/37	92/11	73/27	85/44	62/47	20/81	75/52	67/71	60/38	0/56	53/31

* The ratio of modeled GBO_3 to alternative GBO_3 was 1.
** Poor data capture in June for Pinedale.

show negative ratios during the summer, indicating large over predictions of anthropogenic O_3.

3.5. Attributing monthly model error to source contribution

We attributed site-specific monthly under and over predictions to the GBO_3 or anthropogenic O_3 components by combining entries in Tables 2 and 3 into Table 4, which shows months with under and over predictions. For almost all high-elevation sites, the model under predicted in the spring months when the above-median MDA8 GBO_3 coincided with diagnosed STT-S events. Given the relatively small spring anthropogenic contributions at these sites, it is likely that under estimates were associated with GBO_3. For some urban sites (Boston, Dallas, Detroit, New York, and Sacramento), the model also under predicted during the spring when higher GBO_3 coincided with diagnosed STT-S events; for others (Atlanta, Baltimore, Chicago, Cleveland, Georgia Station, Houston, Philadelphia, St. Louis, and Washington DC), spring over predictions occurred when higher GBO_3 coincided with STT-S events. For urban sites with higher spring anthropogenic influences, it was more likely that over predictions were associated with anthropogenic O_3.

Table 5 summarizes the relative occurrence of diagnosed STT-S events with respect to MDA8 GBO_3 above and below the 1:1 scatter plot line (as shown in Figs. 3–5) for all 23 sites. For each month, Table 5 displays two sets of numbers: the left number represents the fraction of days when STT-S >0 and MDA8 GBO_3 was below the 1:1 line; the right number represents the fraction of days when STT-S $=0$ and MDA8 GBO_3 was above the 1:1 line. The numbers in blue (red) identify the specific months when STT-S was (not) associated with MDA8 GBO_3 below (above) the 1:1 line. At high-elevation sites during all seasons, and several urban sites in spring, STT-S tended to be associated with under estimates of GBO_3. At many of the urban sites, the STT-S summer contribution was not as large as during the spring and over predictions of anthropogenic O_3 were likely responsible, as indicated by the right-hand percentages. Where modeled over predictions were more clearly the result of anthropogenic production (often with biogenic contributions), the heightened chemical reactivity in those environments likely also accelerated GBO_3 decay which possibly contributed to the over prediction by providing a large source of oxidants.

3.6. Characterizing EIB O_3

EIB O_3 mostly consists of GBO_3 because the continental natural O_3 contributions estimated from the OSAT source-apportionment model were small and mostly associated with the anthropogenic component. Western high-elevation EIB (scaled for hourly model error) contributed a large percentage of the observed total spring, fall, and winter O_3 (Table S4). Summer EIB contributions were lower but still provided a significant fraction. EIB also contributed a higher fraction to observed total O_3 at lower elevation sites during spring, fall, and winter although less so than at high-elevation sites.

Fig. 6 and S2 plot the modeled contributions of hourly EIB to the total O_3 frequency distribution (black curve) over the entirety of 2006. The EIB and anthropogenic components reflect the maximum of the error-adjusted hourly EIB O_3 range. For example, the estimated EIB O_3 at Yellowstone NP contributes $>75\%$ to total O_3 (Fig. 6a); at Denver the EIB O_3 contributes $>50\%$ (Fig. 6b) and at Atlanta, the EIB O_3 contributes $>50\%$ of mid-range total O_3 (30–50 ppb) with a lower contribution outside this range as result of dominant local anthropogenic influences (Fig. 6c).

Fig. 7 plots daily error-adjusted ranges of hourly EIB O_3 for the Yellowstone NP, Denver, and Atlanta sites. At these and other sites (Fig. S3), a higher simulated spring, fall, and winter EIB O_3 occurs than in the summer when peak photochemical activity suppresses

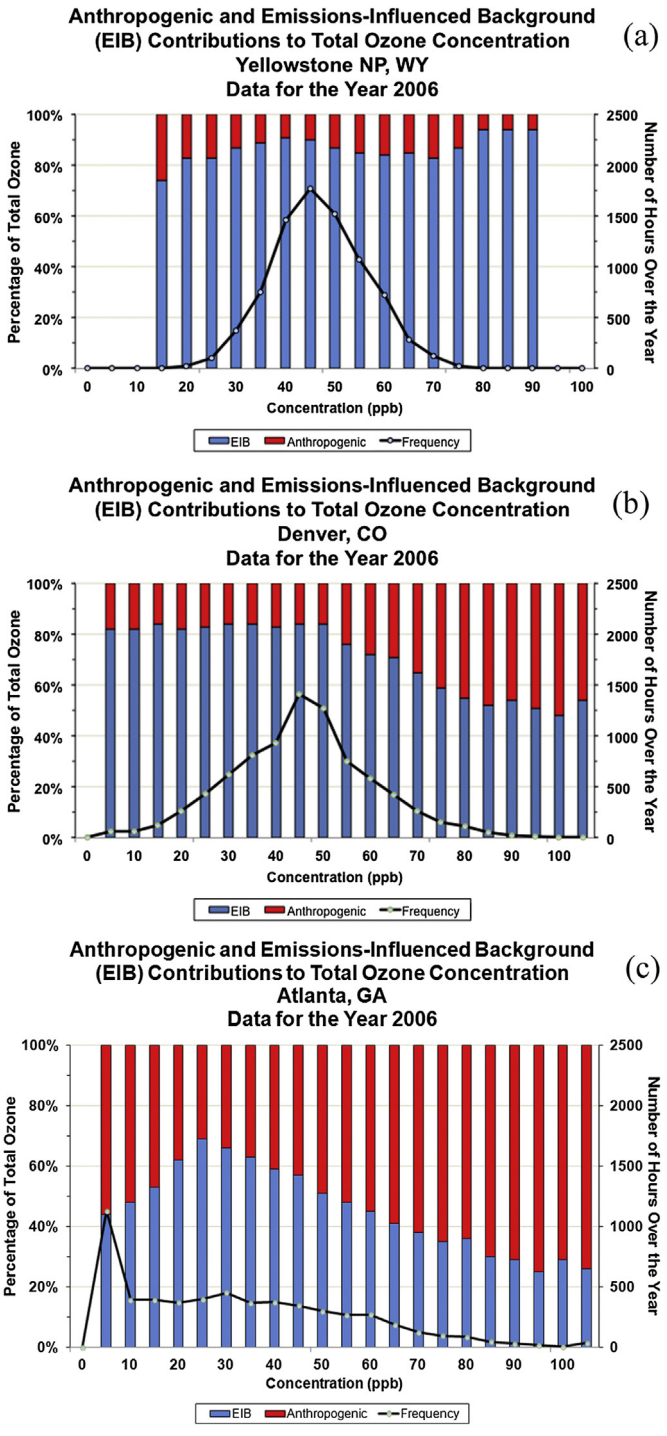

Fig. 6. Binned (5 ppb) frequency distribution of observed hourly total O_3 (black curve; right axis) and average relative binned contributions of maximum hourly EIB and anthropogenic O_3 (bars; left axis) for a) Yellowstone NP, b) Denver, and c) Atlanta.

background O_3. At some western high-elevation sites, the pattern is less discernible given the high EIB O_3 concentrations that occur throughout the year.

4. Discussion and conclusion

The modeling system employed in this study includes dynamic STT processes that explicitly drive the tagged stratospheric

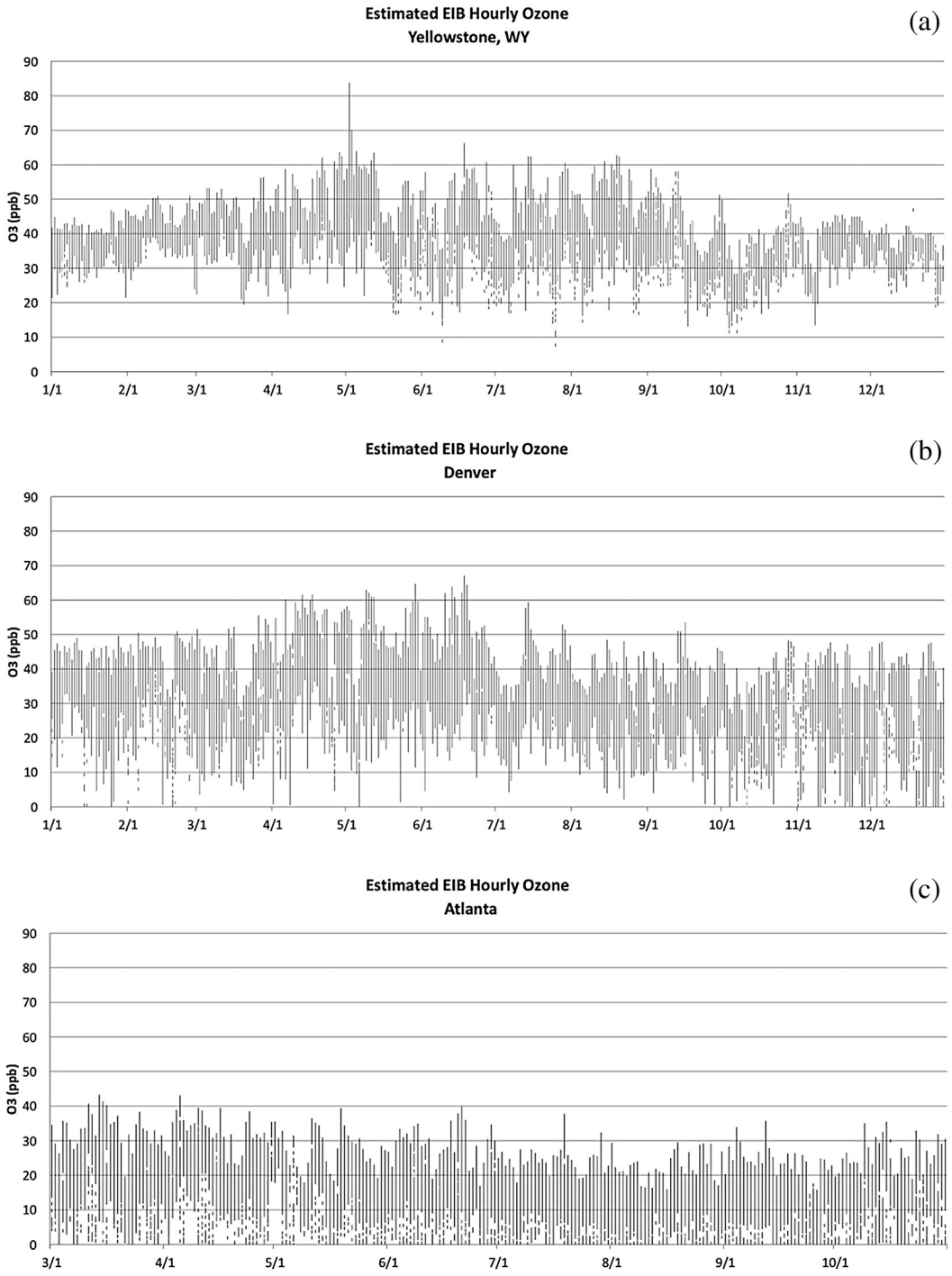

Fig. 7. Time series showing the estimated daily uncertainty range in hourly estimated EIB O_3 for a) Yellowstone NP, b) Denver, and c) Atlanta sites.

O_3 component within the CAMx North American modeling domain and contribute to the global tropospheric O_3 component that enters the CAMx domain via boundary conditions from GEOS-Chem. This approach is consistent with other tagging approaches used in global models for quantifying source contributions (Fiore et al., 2002; Murazaki and Hess, 2006; Wu et al., 2009; Emmons et al., 2010; Wild et al., 2012). Our source apportionment method uses a simple and arbitrary splitting of the troposphere and stratosphere at 10 km on the CAMx domain boundary that we considered representative over the entire domain for the annual simulation. However, this split was likely too high for many periods, especially the winter and spring when the stratosphere can drop to as low as 6–7 km in deep low-pressure waves. Consequently, our stratospheric estimates were likely biased low, while our global tropospheric O_3 estimates included some stratospheric O_3 to a varying degree depending on location and season. Indeed, our CAMx-derived estimates of the stratospheric contribution to surface O_3 were smaller than suggested by recent global modeling studies, where Zhang et al. (2011) employed a tagging approach to track stratospheric O_3

and where Lin et al. (2012) explicitly modeled the stratosphere to analyze event specific STT-S. By combining stratospheric and global tropospheric O_3 in our analyses of total GBO_3, our results compensated for the underestimated CAMx-derived stratospheric contribution to surface O_3 by including STT contributions to global tropospheric O_3.

Both high- and low-elevation sites across the US exhibited spring, fall, and winter GBO_3 concentrations that were higher than in the summer months. GBO_3 was dominant throughout the year at high-elevation sites, even with lower contributions in the summer months. A summer suppression of GBO_3 was associated in part to heightened chemical decay of background O_3 as reactivity increased with local anthropogenic and natural emissions.

Spring, fall, and winter STT-S events frequently coincide with "enhanced" surface O_3 at both high- and low-elevation monitoring sites (Lefohn et al., 2011, 2012). Stratospheric O_3 also appears to influence seasonal patterns of estimated GBO_3. However, long-range Asian transport also contributes to these spring GBO_3 patterns. In particular, during the spring and early summer, Lin et al. (2012) reported that western US spring and early summer background O_3 is routinely elevated by stratospheric O_3 with STT-S contributing more than O_3 generated from Asian emissions. Similar findings were reported by Ambrose et al. (2011) for the Mount Bachelor area in Oregon. Our results support the Lin et al. (2012) findings in that our GBO_3 seasonal patterns are associated with STT processes. For areas east of the Intermountain West, Lin et al. (2012) reported that Asian emissions have minimal impact.

Emery et al. (2012) indicate that their modeled STT effects on surface O_3 were underestimated on an event basis and conclude that wildfires, lightning NO_x, and stratospheric intrusions contribute substantial uncertainty to estimated background O_3. At the western high-elevation sites that experience low anthropogenic influence during the spring, model under prediction tendencies in the current study were associated with systematic underestimation of GBO_3 and that underestimation may have been related to the occurrence of STT events. For urban sites that experience higher spring and summer anthropogenic influence, model over prediction tendencies appear to be associated with over predictions of modeled anthropogenic O_3. Our results at urban sites indicate that STT-S tended to be associated with spring GBO_3 under estimates, while during the summer modeled overestimates of anthropogenic and biogenic interactions accelerated GBO_3 decay, which may have in turn contributed a large source of oxidants.

Our EIB O_3 estimates are presented as an hourly range, which reflects a proportion of the total model uncertainty (observed O_3 − estimated O_3). The uncertainty in EIB O_3 is mostly associated with under or over predictions of GBO_3 because the natural component remained small The GBO_3 patterns described above thus translate to similar patterns for EIB O_3. Based on the tendency for the models to underestimate STT processes, we conclude that the upward-adjusted values of the hourly EIB concentration range are preferable, especially during the spring at high-elevation sites, to an average or median value of the hourly range.

EIB O_3 contributes a major portion to estimated total O_3 for most sites in our analysis, especially during the spring (Table S4). At the western high-elevation sites, the contributions of EIB to total O_3 were usually greater than 70% over the entire year. The eastern high-elevation site at Shenandoah NP experienced contributions of EIB to total O_3 greater than 50% for January–May and October–December. For many of the low-elevation sites, the contributions were 50% and higher during non-summer months (Table S4). For high-elevation sites over the entire annual frequency distribution of total hourly O_3, EIB O_3 contributed more than 50% of total O_3 for Denver, and >75% of total O_3 for Yellowstone NP. In contrast, EIB O_3 contributed less to the upper O_3 concentrations at the more anthropogenically perturbed sites but still >50% of the total O_3 at the mid-range levels (30–50 ppb).

We estimated hourly EIB O_3 for 23 sites based on a model-derived source apportionment technique. We believe that this measure of background O_3 better characterizes how stratospheric, global tropospheric, and natural sources of O_3 are subsequently transported to urban areas and how they contribute to (and are impacted by) local photochemistry. Lacking a direct measure of background O_3, accurate estimates are required to quantify the potential human health and welfare risks and the benefits accrued from proposed emission reductions. These results should provide a better spatial-temporal understanding of current background O_3 concentrations and the attainability of alternative US O_3 standards.

Appendix A. Supplementary data

Supplementary data related to this article can be found at http://dx.doi.org/10.1016/j.atmosenv.2013.11.033

References

Akriditis, D., Zanis, P., Pytharoulis, I., Mavrakis, A., Karacostas, Th, 2010. A deep stratospheric intrusion event down to the earth's surface of the megacity of Athens. Meteorol. Atmos. Phys. 109, 9–18.

Ambrose, J.L., Reidmiller, D.R., Jaffe, D.A., 2011. Causes of high O_3 in the lower free troposphere over the Pacific Northwest as observed at the Mt. Bachelor Observatory. Atmos. Environ. 45, 5302–5315.

Cooper, O.R., Stohl, A., Hübler, G., Hsie, E.Y., Parrish, D.D., Tuck, A.F., Kiladis, G.N., Oltmans, S.J., Johnson, B.J., Shapiro, M., Moody, J.L., Lefohn, A.S., 2005. Direct transport of mid-latitude stratospheric ozone into the lower troposphere and marine boundary layer of the tropical Pacific Ocean. J. Geophys. Res. 110, D23310. http://dx.doi.org/10.1029/2005JD005783.

Cooper, O.R., Oltmans, S.J., Johnson, B.J., Brioude, J., Angevine, W., Trainer, M., Parrish, D.D., Ryerson, T.R., Pollack, I., Cullis, P.D., Ives, M.A., Tarasick, D.W., Al-Saadi, J., Stajner, I., 2011. Measurement of western U.S. baseline ozone from the surface to the tropopause and assessment of downwind impact regions. J. Geophys. Res. 116, D00V03. http://dx.doi.org/10.1029/2011JD016095.

Cristofanelli, P., Bonasoni, P., Tositti, L., Bonafè, U., Calzolari, F., Evangelisti, F., Sandrini, S., Stohl, A., 2006. A 6-year analysis of stratospheric intrusions and their influence on ozone at Mt. Cimone (2165 m above sea level). J. Geophys. Res. 111, D03306. http://dx.doi.org/10.1029/2005JD006553.

Cristofanelli, P., Bracci, A., Sprenger, M., Marinoni, A., Bonafè, U., Calzolari, F., Duchi, R., Laj, P., Pichon, J.M., Roccato, F., Venzac, H., Vuillermoz, E., Bonasoni, P., 2010. Tropospheric ozone variations at the Nepal Climate Observatory-Pyramid (Himalayas, 5079 m a.s.l.) and influence of deep stratospheric intrusion events. Atmos. Chem. Phys. 10, 6537–6549. http://dx.doi.org/10.5194/acp-10-6537-2010.

Danielsen, E.F., 1968. Stratospheric-tropospheric exchange based on radioactivity, ozone and potential vorticity. J. Atmos. Sci. 25, 502–518.

Danielsen, E.F., 1975. The nature of transport processes in the stratosphere. In: Grobecker, A.J. (Ed.), The Natural Stratosphere of 1974, CIAP Monograph I. US Dept. of Transp., Washington, D.C., pp. 6-12–6-22. DOT-TST-75-51.

Danielsen, E.F., Mohnen, V.A., 1977. Project Duststorm report: ozone transport, in situ measurements and meteorological analyses of tropopause folding. J. Geophys. Res. 82, 5867–5877.

Davies, T.D., Schuepbach, E., 1994. Episodes of high ozone concentrations at the earth's surface resulting from transport down from the upper troposphere/lower stratosphere: a review and case studies. Atmos. Environ. 28, 53–68.

Dunker, A.M., Yarwood, G., Ortmann, J.P., Wilson, G.M., 2002. Comparison of source apportionment and source sensitivity of ozone in a three-dimensional air quality model. Environ. Sci. Technol. 36, 2953–2964.

Emery, C., Jung, J., Downey, N., Johnson, J., Jimenez, M., Yarwood, G., Morris, R., 2012. Regional and global modeling estimates of policy relevant background ozone over the United States. Atmos. Environ. 47, 206–217.

Emmons, L.K., Walters, S., Hess, P.G., Lamarque, J.-F., Pfister, G.G., Fillmore, D., Granier, C., Guenther, A., Kinnison, D., Laepple, T., Orlando, J., Tie, X., Tyndall, G., Wiedinmyer, C., Baughcum, S.L., Kloster, S., 2010. Description and evaluation of the model for ozone and related chemical tracers, version 4 (MOZART-4). Geosci. Model Dev. 3, 43–67. http://dx.doi.org/10.5194/gmd-3-43-2010.

ENVIRON, 2011. User's Guide: Comprehensive Air Quality Model with Extensions (CAMx), Version 5.4. Prepared by ENVIRON International Corporation, Novato, CA. Available at: www.camx.com.

Fiore, A.M., Jacob, D.J., Bey, I., Yantosca, R.M., Field, B.D., Fusco, A.C., Wilkinson, J.G., 2002. Background ozone over the United States in summer: origin, trend, and contribution to pollution episodes. J. Geophys. Res. 107 (D15), 4275. http://dx.doi.org/10.1029/2001JD000982.

Fiore, A., Jacob, D.J., Liu, H., Yantosca, R.M., Fairlie, T.D., Li, Q., 2003. Variability in surface ozone background over the United States: implications for air quality

policy. J. Geophys. Res. 108 (D24), 4787. http://dx.doi.org/10.1029/2003JD003855.
GMAO, 2013. NASA Goddard Space Flight Center, GMAO Products. Web site: http://gmao.gsfc.nasa.gov/products/.
Haagenson, P.L., Shapiro, M.A., Middleton, P., Laird, A.R., 1981. A case study relating high ground level ozone to enhanced photochemistry and isentropic transport from the stratosphere. J. Geophys. Res. 86, 5231–5237.
Harvard, 2013. GEOS-chem On-line Documentation. Available at: http://acmg.seas.harvard.edu/geos/index.html.
Hocking, W.K., Carey-Smith, T., Tarasick, D.W., Argall, P.S., Strong, K., Rochon, Y., Zawadzki, I., Taylor, P.A., 2007. Detection of stratospheric ozone intrusions by wind profiler radars. Nature 450, 281–284.
Junge, C., 1962. Global ozone budget and exchange between stratosphere and troposphere. Tellus 14, 363–377.
Koo, B., Chien, C.J., Tonnesen, G., Morris, R., Johnson, J., Sakulyanontvittaya, T., Piyachaturawat, P., Yarwood, G., 2010. Natural emissions for regional modeling of background ozone and particulate matter and impacts on emissions control strategies. Atmos. Environ. 44, 2372–2382.
Lamarque, J.-F., Hess, P.G., 1994. Cross-tropopause mass exchange and potential vorticity budget in a simulated tropopause folding. J. Atmos. Sci. 51, 2246–2269.
Langford, A.O., Aikin, K.C., Eubank, C.S., Williams, E.J., 2009. Stratospheric contribution to high surface ozone in Colorado during springtime. Geophys. Res. Lett. 36, L12801. http://dx.doi.org/10.1029/2009GL038367.
Langford, A.O., Brioude, J., Cooper, O.R., Senff, C.J., Alvarez II, R.J., Hardesty, R.M., Johnson, B.J., Oltmans, S.J., 2012. Stratospheric influence on surface ozone in the Los Angeles area during late spring and early summer of 2010. J. Geophys. Res. 117, D00V06. http://dx.doi.org/10.1029/2011JD016766.
Ludwig, F.L., Reiter, E., Shelar, E., Johnson, W.B., 1977. The Relation of Oxidant Levels to Precursor Emissions and Meteorological Features. In: Analysis and Findings, vol. I. U.S. Environmental Protection Agency, Office of Air Quality Planning and Standards/NTIS, Research Triangle Park, NC/Springfield, VA report no. EPA-450/3-77-022a. Available from: PB-275 001.
Lefohn, A.S., Oltmans, S.J., Dann, T., Singh, H.B., 2001. Present-day variability of background ozone in the lower troposphere. J. Geophys. Res. 106 (D9), 9945–9958. http://dx.doi.org/10.1029/2000JD900793.
Lefohn, A.S., Wernli, H., Shadwick, D., Limbach, S., Oltmans, S.J., Shapiro, M., 2011. The importance of stratospheric-tropospheric transport in affecting surface ozone concentrations in the western and northern tier of the United States. Atmos. Environ. 45, 4845–4857.
Lefohn, A.S., Wernli, H., Shadwick, D., Oltmans, S.J., Shapiro, M., 2012. Quantifying the frequency of stratospheric-tropospheric transport affecting enhanced surface ozone concentrations at high- and low-elevation monitoring sites in the United States. Atmos. Environ. 62, 646–656.
Lin, M., Fiore, A.M., Cooper, O.R., Horowitz, L.W., Langford, A.O., Levy II, H., Johnson, B.J., Naik, V., Oltmans, S.J., Senff, C.J., 2012. Springtime high surface ozone events over the western United States: quantifying the role of stratospheric intrusions. J. Geophys. Res. 117, D00V22. http://dx.doi.org/10.1029/2012JD018151.
McDonald-Buller, E.C., Allen, D.T., Brown, N., Jacob, D.J., Jaffe, D., Kolb, C.E., Lefohn, A.S., Oltmans, S., Parrish, D.D., Yarwood, G., Zhang, L., 2011. Establishing policy relevant background (PRB) ozone concentrations in the United States. Environ. Sci. Technol. 45, 9484–9497. http://dx.doi.org/10.1021/es2022918.
Mueller, S.F., Mallard, J.W., 2011. Contributions of natural emissions to ozone and PM2.5 as simulated by the Community Multiscale Air Quality (CMAQ) model. Environ. Sci. Technol. 45, 4817–4823. http://dx.doi.org/10.1021/es103645m.
Murazaki, K., Hess, P., 2006. How does climate change contribute to surface ozone change over the United States? J. Geophys. Res. 111 http://dx.doi.org/10.1029/2005JD005873.
Oltmans, S.J., Lefohn, A.S., Harris, J.M., Shadwick, D., 2008. Background ozone levels of air entering the west coast of the US and assessment of longer-term changes. Atmos. Environ. 42, 6020–6038.
Ordóñez, C., Brunner, D., Staehelin, J., Hadjinicolaou, P., Pyle, J.A., Jonas, M., Wernli, H., Prevot, A.S.H., 2007. Strong influence of lowermost stratospheric ozone on lower tropospheric background ozone changes over Europe. Geophys. Res. Lett. 34, L07805. http://dx.doi.org/10.1029/2006GL029113.
Pouliot, G., Pierce, T., Denier van der Gon, H., Schaap, M., Moran, M., Nopmongcol, U., 2012. Comparing emission inventories and model-ready emission datasets between Europe and North America for the AQMEII project. Atmos. Environ. 53, 4–14. http://dx.doi.org/10.1016/j.atmosenv.2011.12.041.
Rao, S.T., Galmarini, S., Puckett, K., 2011. Air Quality Model Evaluation International Initiative (AQMEII): advancing state-of-science in regional photochemical modeling and its applications. Bull. Am. Meteorol. Soc. 92, 23–30. http://dx.doi.org/10.1175/2010BAMS3069.1.
Reed, R.J., 1955. A study of a characteristic type of upper level frontogenesis. J. Meteorol. 12, 226–237.
Reidmiller, D.R., Fiore, A.M., Jaffe, D.A., Bergmann, D., Cuvelier, C., Dentener, F.J., Duncan, B.N., Folberth, G., Gauss, M., Gong, S., Hess, P., Jonson, J.E., Keating, T., Lupu, A., Marmer, E., Park, R., Schultz, M.G., Shindell, D.T., Szopa, S., Vivanco, M.G., Wild, O., Zuber, A., 2009. The influence of foreign vs. North American emissions on surface ozone in the US. Atmos. Chem. Phys. 9, 5027–5042.
Schuepbach, E., Davies, T.D., Massacand, A.C., 1999. An unusual springtime ozone episode at high elevation in the Swiss Alps: contributions both from cross-tropopause exchange and from the boundary layer. Atmos. Environ. 33, 1735–1744.
Shapiro, M.A., 1980. Turbulent mixing within tropopause folds as a mechanism for the exchange of chemical constituents between the stratosphere and troposphere. J. Atmos. Sci. 37, 994–1004.
Stohl, A., Spichtinger-Rakowsky, N., Bonasoni, P., Feldmann, H., Memmesheimer, M., Scheel, H.E., Trickl, T., Hübener, S., 2000. The influence of stratospheric intrusions on alpine ozone concentrations. Atmos. Environ. 34, 1323–1354.
US Environmental Protection Agency, US EPA, June 1996. Review of National Ambient Air Quality Standards for Ozone - Assessment of Scientific and Technical Information. OAQPS Staff Paper. EPA-452/R-96–007. Office of Air Quality Planning and Standards/US Environmental Protection Agency, Research Triangle Park, NC.
US Environmental Protection Agency, US EPA, February 2006. Air Quality Criteria for Ozone and Related Photochemical Oxidants. Report Nos. EPA/600/R-05/004af. Office of Research and Development/US Environmental Protection Agency, Research Triangle Park, NC.
US Environmental Protection Agency, US EPA, July 2012. Health Risk and Exposure Assessment for Ozone. EPA/452/P-12-001. Office of Air Quality Planning and Standards, Research Triangle Park, NC. First External Review Draft.
US Environmental Protection Agency, US EPA, February 2013. Integrated Science Assessment for Ozone and Related Photochemical Oxidants. EPA/600/R-10/076F. Office of Research and Development, Research Triangle Park, NC.
Vautard, R., Moran, M., Solazzo, E., Gilliam, R., Matthias, V., Bianconi, R., Chemel, C., Ferreira, J., Geyer, B., Hansen, A., Jericevic, A., Prank, M., Segers, A., Silver, J., Werhahn, J., Wolke, R., Rao, S.T., Galmarini, S., 2012. Evaluation of the meteorological forcing used for the Air Quality Model Evaluation International Initiative (AQMEII) air quality simulations. Atmos. Environ. 53, 15–37. http://dx.doi.org/10.1016/j.atmosenv.2011.10.065.
Wang, H., Jacob, D.J., Le Sager, P., Streets, D.G., Park, R.J., Gilliland, A.B., van Donkelaar, A., 2009. Surface ozone background in the United States: Canadian and Mexican pollution influences. Atmos. Environ. 43, 1310–1319.
Wernli, H., Davies, H.C., 1997. A Lagrangian-based analysis of extratropical cyclones. I: the method and some applications. Q. J. R. Meteorol. Soc. 123, 467–489.
Wernli, H., Bourqui, M., 2002. A Lagrangian "one-year climatology" of (deep) cross-tropopause exchange in the extratropical northern hemisphere. J. Geophys. Res. 107 (D2), 4021. http://dx.doi.org/10.1029/2001JD000812.
Wild, O., Fiore, A.M., Shindell, D.T., Doherty, R.M., Collins, W.J., Dentener, F.J., Schultz, M.G., Gong, S., MacKenzie, I.A., Zeng, G., Hess, P., Duncan, B.N., Bergmann, D.J., Szopa, S., Jonson, J.E., Keating, T.J., Zuber, A., 2012. Modelling future changes in surface ozone: a parameterized approach. Atmos. Chem. Phys. 12, 2037–2054. http://dx.doi.org/10.5194/acp-12-2037-2012.
Wu, S., Duncan, B.N., Jacob, D.J., Fiore, A.M., Wild, O., 2009. Chemical nonlinearities in relating intercontinental ozone pollution to anthropogenic emissions. Geophys. Res. Lett. 36, L05806. http://dx.doi.org/10.1029/2008GL036607.
Yarwood, G., Rao, S.T., Yocke, M., Whitten, G.Z., 2005. Updates to the Carbon Bond Chemical Mechanism: CB05. Final Report prepared for US Environmental Protection Agency, Research Triangle Park, NC. Available at: http://www.camx.com/publ/pdfs/CB05_Final_Report_120805.pdf.
Zhang, L., Jacob, D.J., Downey, N.V., Wood, D.A., Blewitt, D., Carouge, C.C., van Donkelaar, A., Jones, D.B.A., Murray, L.T., Wang, Y., 2011. Improved estimate of the policy-relevant background ozone in the United States using the GEOS-Chem global model with 1/2° × 2/3° horizontal resolution over North America. Atmos. Environ. 45, 6769–6776.